JACS
JOURNAL OF THE AMERICAN CHEMICAL SOCIETY

Article

pubs.acs.org/JACS

Promoting Active Species Generation by Plasmon-Induced Hot-Electron Excitation for Efficient Electrocatalytic Oxygen Evolution

Guigao Liu,[†,‡] Peng Li,[‡] Guixia Zhao,[‡] Xin Wang,[§,∥] Jintao Kong,[⊥] Huimin Liu,[‡] Huabin Zhang,*[,‡] Kun Chang,[‡] Xianguang Meng,[‡] Tetsuya Kako,[‡] and Jinhua Ye*[,†,‡,§,∥]

[†]Graduate School of Chemical Science and Engineering, Hokkaido University, Sapporo 060-8628, Japan

[‡]International Center for Materials Nanoarchitectonics (WPI-MANA), National Institute for Materials Science (NIMS), Tsukuba, Ibaraki 305-0044, Japan

[§]TU-NIMS Joint Research Center, School of Materials Science and Engineering, Tianjin University, Tianjin 300072, China

[∥]Collaborative Innovation Center of Chemical Science and Engineering (Tianjin), Tianjin 300072, China

[⊥]Key Laboratory of Optoelectronic Materials Chemistry and Physics, Fujian Institute of Research on the Structure of Matter, Chinese Academy of Sciences, Fuzhou 350002, China

Supporting Information

ABSTRACT: Water splitting represents a promising technology for renewable energy conversion and storage, but it is greatly hindered by the kinetically sluggish oxygen evolution reaction (OER). Here, using Au-nanoparticle-decorated $Ni(OH)_2$ nanosheets [$Ni(OH)_2$–Au] as catalysts, we demonstrate that the photon-induced surface plasmon resonance (SPR) excitation on Au nanoparticles could significantly activate the OER catalysis, specifically achieving a more than 4-fold enhanced activity and meanwhile affording a markedly decreased overpotential of 270 mV at the current density of 10 mA cm^{-2} and a small Tafel slope of 35 mV dec^{-1} (no *iR*-correction), which is much better than those of the benchmark IrO_2 and RuO_2, as well as most Ni-based OER catalysts reported to date. The synergy of the enhanced generation of $Ni^{III/IV}$ active species and the improved charge transfer, both induced by hot-electron excitation on Au nanoparticles, is proposed to account for such a markedly increased activity. The SPR-enhanced OER catalysis could also be observed over cobalt oxide (CoO)–Au and iron oxy-hydroxide (FeOOH)–Au catalysts, suggesting the generality of this strategy. These findings highlight the possibility of activating OER catalysis by plasmonic excitation and could open new avenues toward the design of more-energy-efficient catalytic water oxidation systems with the assistance of light energy.

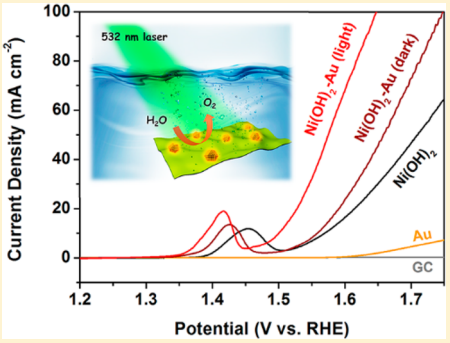

1. INTRODUCTION

Economic and environmental concerns raised by the extensive use of fossil fuels have made alternative energy sources more attractive.[1] Electricity-driven or photodriven water splitting to produce hydrogen and oxygen gases (i.e., $2H_2O \rightarrow 2H_2 + O_2$) provides a promising pathway for renewable energy conversion and storage.[1a,2] However, this process of splitting water usually suffers from significant efficiency loss and high overpotentials (η) due to the sluggish kinetics of the oxidative half-reaction [i.e., oxygen evolution reaction (OER), $2H_2O \rightarrow 4H^+ + O_2 + 4e^-$ in acid and $4OH^- \rightarrow 2H_2O + O_2 + 4e^-$ in base].[3] To accelerate the OER reaction, reduce the overpotential, and therefore improve the overall energy efficiency, an appropriate electrocatalyst is critical.[3b,4] Recently, earth-abundant transition-metal-based (like Ni, Co, and Fe) materials have been considerably developed as OER catalysts due to their great potential for OER catalysis and high stability under alkaline conditions as well as their environmentally benign nature.[4,5] During electrochemical processes, the transition-metal cations in materials generally undergo progressive oxidation from low valence states to high valence states prior to the onset of the OER reaction (for example, Ni^{II} to $Ni^{III/IV}$,[5d,6] Co^{III} to Co^{IV},[5e,g,7] and Fe^{III} to Fe^{IV} [8]). This phenomenon makes one reasonably aware that the highly oxidative metal cations are required to catalyze OER and that they might be active sites for OER catalysts.[5g,6b] It appears that the performance of the transition-metal-based OER catalysts could be promoted by increasing the population of high oxidation metal species in materials.[3e,6d,9] However, the exploration of a facile and effective approach to achieve this goal still battles huge challenges, thereby greatly hindering the further development of such kinds of promising OER catalysts for practical applications.

As an abundant and clean energy source, light has been widely applied as a driving force for chemical synthesis, which represents a promising technology for light energy conversio-

Received: February 11, 2016
Revised: May 19, 2016
Published: July 5, 2016

DOI: 10.1021/jacs.6b05190
J. Am. Chem. Soc. 2016, 138, 9128–9136

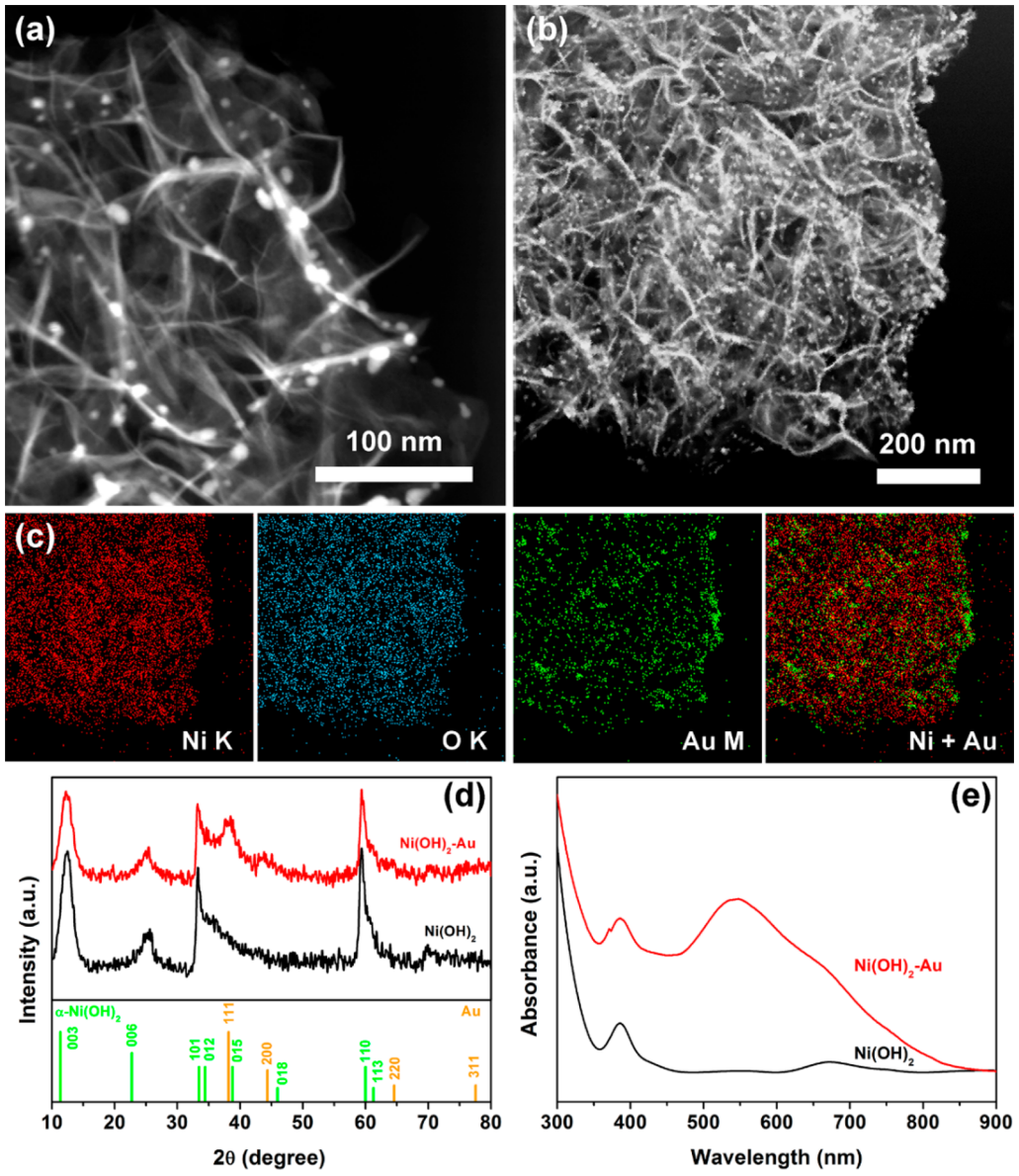

Figure 1. General characterization of the $Ni(OH)_2$–Au nanostructures. (a, b) HAADF-STEM images of $Ni(OH)_2$–Au hybrid catalysts. The Au nanoparticles can be identified by their higher contrast. (c) 2D element mapping images of Ni, O, and Au in the area shown in part b. (d) XRD patterns and (e) UV–vis absorption spectra of original $Ni(OH)_2$ nanosheets and $Ni(OH)_2$–Au hybrids.

n.[1a,2f] Among the considerable advances, the surface plasmon resonance (SPR) effect observed on the illuminated plasmonic metal nanostructures (such as noble Au and Ag nanoparticles) attracts increasing attention because it is capable of efficiently harvesting and converting the energy from light to chemical energy through plasmonic excitation.[10] During the process, energetic electrons (also referred to as "hot electrons") will be excited by the resonant photons and then transferred to the nearby conductive or semiconductive substrates, simultaneously retaining energetic holes on the surface of plasmonic nanostructures for oxidation reactions or capturing foreign electrons.[11] Such a SPR excitation induced photovoltaic effect enables light energy conversion and, importantly, inspires us to reasonably hypothesize that it might be able to contribute additionally to the preceding electricity-driven generation of high-valence OER active metal species in the transition-metal-based catalysts and subsequently to facilitate water oxidation. Simultaneously, hybridizing the transition-metal-based OER catalysts with plasmonic noble-metal nanostructures could actually cause an intrinsic small electron transfer from the catalysts to the noble metals because of the high electronegativity of the latter (for example, Au is the most electronegative metal).[5g,6b] This is believed to be also beneficial for the oxidation of transition-metal cations in catalysts.[5g,6b] Therefore, an effective synergy, between such an intrinsic electronic charge transfer interaction and the above-mentioned SPR photovoltaic effect, for enhanced OER active metal species formation and increased OER catalysis is highly anticipated in the transition-metal-based OER catalysts modified with plasmonic metal nanostructures. Additionally, to the best of our knowledge, the investigation on the plasmon-assisted electrocatalytic water oxidation behaviors is still at the early stage, and few reports have emerged that utilize the plasmon–electricity coupling effect for efficient OER catalysis.

In this study, the layer-structured nickel hydroxide [$Ni(OH)_2$] nanosheets were prepared and intentionally chosen as

DOI: 10.1021/jacs.6b05190
J. Am. Chem. Soc. 2016, 138, 9128–9136

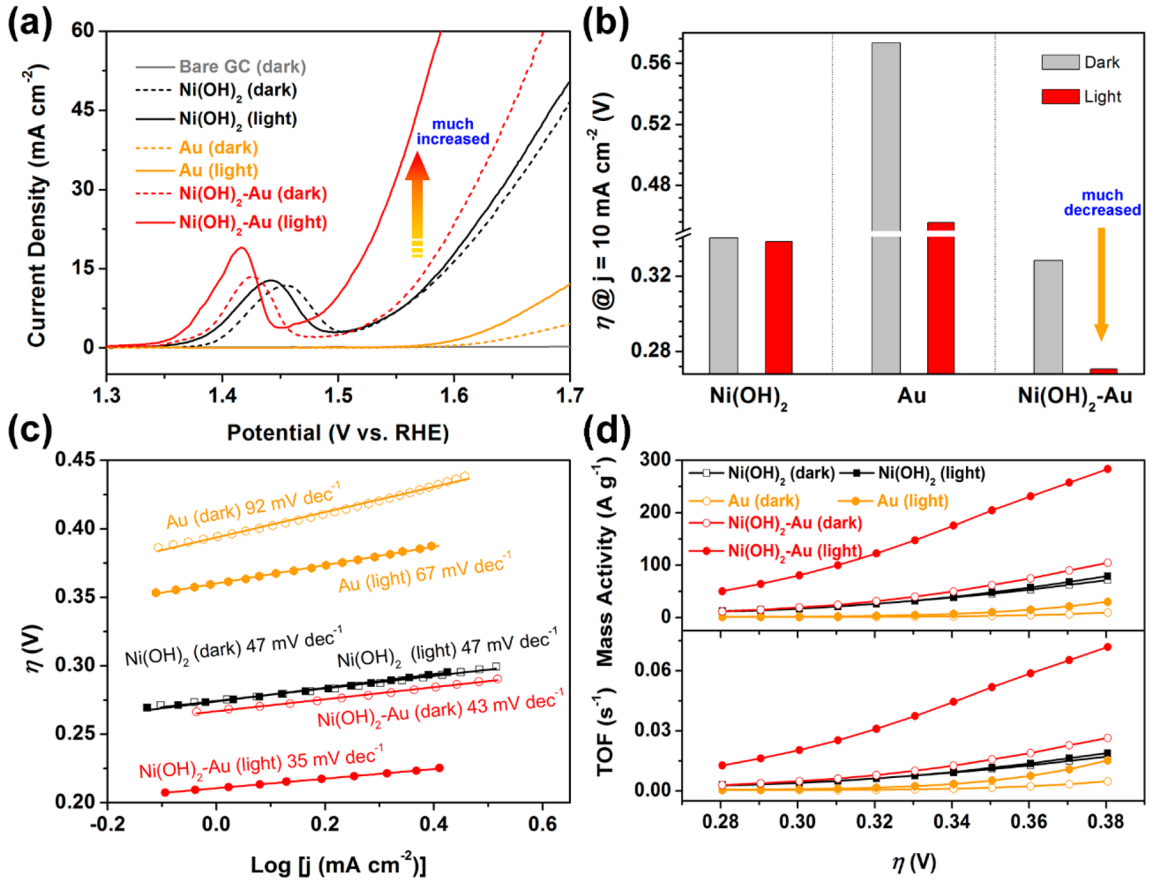

Figure 2. Electrochemical performances of $Ni(OH)_2$–Au hybrid catalysts and control samples measured in 1.0 M KOH electrolyte with and without light irradiation (532 nm laser). (a) OER polarization curves (without *iR*-correction). Scan rate was 10 mV s^{-1}. (b) Comparison of overpotentials (η) required for a 10 mA cm^{-2} current density over $Ni(OH)_2$–Au hybrid catalysts and control samples with and without light irradiation. (c) Tafel plots of catalysts [for $Ni(OH)_2$ and $Ni(OH)_2$–Au catalysts, Tafel plots were calculated using the cathodic sweep from the corresponding cyclic voltammetry curves to avoid the interference of the $Ni(OH)_2$ oxidation peak]. (d) Mass activities (top) and TOF values (bottom) of catalysts at different overpotentials.

the primary model OER catalysts because of the intrinsic good water oxidation potential and unique two-dimensional structure.[12] Au nanoparticles were decorated onto the $Ni(OH)_2$ nanosheets [$Ni(OH)_2$–Au] as light-harvesting antennas and plasmon exciter. We for the first time show that the oxygen evolution reaction can be significantly (precisely, a more than 4-fold enhancement) activated by the resonant surface plasmon excitation generated on plasmonic Au nanoparticles through the light harvesting and conversion. Our studies indicate that plasmon-driven hot-electron excitation enhances the charge transfer from $Ni(OH)_2$ nanosheets to Au nanoparticles and greatly facilitates the oxidation of inactive Ni^{II} to active $Ni^{III/IV}$ species, finally allowing for more efficient water oxidation at lower onset potential. Such SPR-excitation-enhanced OER catalysis was also observed over other Au-nanoparticle-loaded transition-metal-based catalysts, such as CoO and FeOOH, reflecting the universality of this strategy. These findings provide an insight into the activation of oxygen evolution catalysis through electron withdrawing or donating induced by the plasmonic excitation on illuminated metal nanostructures.

2. RESULTS

$Ni(OH)_2$ nanosheets were first prepared through a modified solvothermal system,[12] and their electron microscope characterizations are shown in Figure S1 [Supporting Information (SI)], where the silklike features of the two-dimensional (2D) nanosheets are clearly evident. Au nanoparticles with an average diameter of 4.8 nm were also synthesized by reduction of $HAuCl_4$ with $NaBH_4$ (see Figure S2, SI). Since the $Ni(OH)_2$ nanosheets and the Au nanoparticles possess the opposite interfacial charges [average ζ-potential is +37.8 mV for $Ni(OH)_2$ nanosheets, and −34.2 mV for Au nanoparticles; Figure S3, SI], they would be spontaneously assembled through the electrostatic interaction in the solution, which finally resulted in the formation of $Ni(OH)_2$–Au hybrid OER catalysts. Figures 1a and S4a (SI) respectively present the high-angle annular dark-field scanning transmission electron microscopy (HAADF-STEM) and the scanning electron microscopy (SEM) images of the as-prepared sample. It is clear that the Au nanoparticles were homogeneously dispersed on the surface of silklike $Ni(OH)_2$ nanosheets (the bright spots in the STEM image indicate the Au nanoparticles). The high-resolution TEM (HRTEM) images displayed in Figure S4b,c (SI) were taken from a part of the $Ni(OH)_2$–Au hybrids and confirm the close interfacial contact between Au nanoparticles and $Ni(OH)_2$ nanosheets, which is believed to be advantageous for electron transfer.[13] Meanwhile, the observed two distinct sets of lattice fringes in Figure S4c (SI) could be assigned to hexagonal α-$Ni(OH)_2$ and fcc Au, respectively. Figure 1b shows the STEM image of a giant $Ni(OH)_2$–Au assembly, and the corresponding elemental mappings are also depicted (Figure 1c), from which the uniform distribution of Au nanoparticles

DOI: 10.1021/jacs.6b05190
J. Am. Chem. Soc. 2016, 138, 9128−9136

Table 1. Comparison of OER Activity for Various Catalysts

catalyst	η at j = 10 mA cm^{-2} (mV)	mass activity at η = 0.30 V (A g^{-1})	Tafel slope (mV dec^{-1})	TOF at η = 0.30 V ($\times 10^{-3}$ s^{-1})
$Ni(OH)_2$–Au (light)	270	80.5	35	20.0
$Ni(OH)_2$–Au (dark)	330	19.3	43	4.9
$Ni(OH)_2$ (light)	338	17.6	47	4.2
$Ni(OH)_2$ (dark)	340	16.7	47	4.0
Au (light)	455	1.8	67	0.9
Au (dark)	573	0.9	92	0.5
IrO_2[18]	330	27.5	52	~14.0
RuO_2[19]	305	NA[a]	60	NA[a]

[a]Not applicable.

over $Ni(OH)_2$ nanosheets is further confirmed. The X-ray diffraction (XRD) patterns [Figures 1d and S5 (SI)] of the as-prepared materials present a consistent result of the HRTEM (Figure S4c, SI); both the hexagonal α-$Ni(OH)_2$ (JCPDS 380715) and cubic Au (JCPDS 01-089-3697) are recognized. Probably due to the loss of some lattice water in the $Ni(OH)_2$ lattice, the (003) and (006) peak positions of α-$Ni(OH)_2$ are shown to be slightly positive-shifted, similar to the reports by others.[12,14] The absorption properties of original $Ni(OH)_2$ nanosheets and $Ni(OH)_2$–Au hybrids were investigated by using a UV–vis spectrophotometer. As shown in Figures 1e and S6 (SI), $Ni(OH)_2$ nanosheets exhibit two small absorption bands at 385 and 670 nm, which can be associated with the d–d transitions of Ni^{II} cations [precisely, $^3A_{2g}(F) \rightarrow {}^3T_{1g}(P)$ for the former and $^3A_{2g}(F) \rightarrow {}^3T_{1g}(F)$ for the latter].[15] After being decorated by Au nanoparticles, a strong photoabsorption peak centered at 540 nm, induced by the surface plasmon excitation of Au,[16] appears in the spectra of $Ni(OH)_2$–Au hybrids, and it is obviously red-shifted as compared with the absorption of the original Au nanoparticles (Figure S6, SI). This indicates the electronic interactions between Au and $Ni(OH)_2$.[11e,17]

The electrocatalytic performances of $Ni(OH)_2$–Au hybrid catalysts toward water oxidation were investigated in O_2-saturated 1.0 M of KOH solutions at room temperature using a standard three-electrode system. As references, the original $Ni(OH)_2$ nanosheets and Au nanoparticles were also tested under identical conditions. Figure 2a records the linear sweep voltammetry (LSV) curves (no *iR*-correction) of all samples at a scan rate of 10 mV s^{-1} (see details in the Experimental Section). As expected, $Ni(OH)_2$–Au exhibits an earlier onset potential [~1.47 V vs reversible hydrogen electrode (RHE)] and higher current density than $Ni(OH)_2$ and Au, suggesting its remarkable activity. However, the most striking result is that, when irradiated with a 532 nm laser nearly corresponding to the maximum SPR absorption of Au nanoparticles, the oxygen evolution is considerably accelerated over $Ni(OH)_2$–Au catalysts, as evidenced by the much lower onset potential and higher current increase rate. Particularly, the overpotential (η) required to achieve the current density of 10 mA cm^{-2}, a metric relevant to solar fuel synthesis, is significantly decreased from 330 to 270 mV (Figure 2b), much lower than the records of the benchmark IrO_2 and RuO_2 catalysts [Tables 1 and S2 (SI)]. To further verify such instant photoresponse of $Ni(OH)_2$–Au to OER catalysis, a LSV scanning with light on and off was first performed. As shown in Figure S7 (SI), an abrupt drop in current is observed expectedly as the laser was removed. Then, we also collected the chronoamperomertic I–t curve of $Ni(OH)_2$–Au under chopped illumination (Figure S8, SI). From the figure, $Ni(OH)_2$–Au exhibits prompt and reproducible current responses to on–off illumination cycles, well supporting the discussion above. In contrast with $Ni(OH)_2$–Au, pure $Ni(OH)_2$ catalysts exhibit negligible enhancement in activity under irradiation (Figure 2a,b). This result pronounces the necessity of Au nanoparticles for the observation of such photoenhancement effect on activity.

The laser-wavelength-dependent water oxidation over $Ni(OH)_2$–Au was further investigated at η = 0.38 V. It can be seen in Figure S9 (SI) that the normalized current density enhancement qualitatively tracks the characteristic absorption of Au nanoparticles. In conjunction with the results above, this phenomenon clearly suggests that the increase in OER performance of $Ni(OH)_2$–Au is mainly derived from the Au SPR excitation.[11c] Other evidence for this conclusion is the observation of a similar enhancement in activity of Au induced by laser irradiation (Figure 2a and b). Here, it is worthy of noted that, in comparison with $Ni(OH)_2$–Au catalysts, Au nanoparticle catalysts exhibit an even larger decrease in the overpotential at 10 mA cm^{-2} upon the laser irradiation (Figure 2b and Table 1). This might be related to the aggregation of Au nanoparticle catalysts, which could generate much enhanced plasmonic excitation due to the strong interparticle electronic interaction (for details, see Figure S10, SI).[20] Figure S11 (SI) shows LSV curves of the samples with different Au loading on $Ni(OH)_2$ nanosheets, and 3.5 wt % is demonstrated to be the optimized value for OER catalysis. This result indicates that the efficient electrocatalytic water oxidation could be realized under light irradiation by grafting OER catalysts with a tiny amount of plasmonic Au nanoparticles. As evidenced by the transient absorption spectroscopic analysis (for details, see Figure S12, SI), the adverse effect on activity upon furthering Au loading is a result of the decrease in plasmonic excitation efficiency. This is probably due to the inefficient electron donation from $Ni(OH)_2$ to Au,[21] and it can be confirmed by the higher binding energy for the Au X-ray photoelectron spectroscopy (XPS) peak of $Ni(OH)_2$–Au(8.9 wt %) than for $Ni(OH)_2$–Au(3.5 wt %) (Figure S13, SI). It is worth noting that, prior to the onset of OER, both the $Ni(OH)_2$–Au and $Ni(OH)_2$ catalysts show the redox peaks around 1.40 to 1.45 V (Figure 2a), which can be assigned to the $Ni^{II}/Ni^{III/IV}$ redox process.[22]

To gain more insight into the effect of light irradiation on the kinetics of OER, a further analysis of the Tafel slope was performed. As seen from Figure 2c, $Ni(OH)_2$–Au exhibits a Tafel slope of 43 mV dec^{-1} in the dark. Importantly, with laser irradiation, the Tafel slope is decreased significantly to 35 mV dec^{-1}. This clearly demonstrates that the kinetics of water oxidation over $Ni(OH)_2$–Au are facilitated by irradiation-induced Au SPR excitation. As expected, such photoactivation on OER is also observed for Au catalysts, but in sharp contrast, it appears to be ineffective for $Ni(OH)_2$ nanosheets (Figure 2c). It needs to be specially noted here that the Tafel slope of

DOI: 10.1021/jacs.6b05190
J. Am. Chem. Soc. 2016, 138, 9128–9136

$Ni(OH)_2$–Au with light irradiation is smaller than (or comparable to) those of previously reported Ni-based OER catalysts and the benchmark IrO_2 and RuO_2 catalysts [Tables 1 and S2 (SI)]. Figure 2d (top) shows the mass activities for various catalysts with and without laser irradiation. All of them exhibit a nearly linear increase with overpotential. In particular, at a quite small overpotential of 0.3 V, the mass activity of $Ni(OH)_2$–Au is boosted from 19.3 to 80.5 A g^{-1} by the activation of Au SPR, which is meanwhile 4.8 and 2.9 times higher than that of $Ni(OH)_2$ (dark) and IrO_2 catalysts, respectively (Table 1). Additionally, enhancements in the turnover frequency (TOF) induced by Au SPR excitation [see Figure 2d (bottom) and Table 1] and in specific activity (based on BET surface area; see Figures S14 and S15, SI) of $Ni(OH)_2$–Au catalysts are also confirmed. All these results evidently suggest that the plasmonic excitation of Au causes significant catalytic activation of $Ni(OH)_2$ nanosheets, which allows the latter to be exploited for more efficient water oxidation at lower onset potential.

3. DISCUSSION

As to Ni-based catalysts, the OER reaction in alkaline electrolyte generally involves the oxidation of Ni^{II} to $Ni^{III/IV}$ [here, the α-$Ni(OH)_2$ (Ni^{II}) is in situ oxidized to NiOOH ($Ni^{III/IV}$); for details, see the SI, Scheme S1, step 1].[6a] Then the highly oxidative $Ni^{III/IV}$ cations are believed to facilitate the formation and the subsequent deprotonation of the key OOH intermediates, finally giving rise to the O_2 evolution (also see the SI, Scheme S1, steps 2–4).[5g,6a–c,e,8c] This mechanism suggests that $Ni^{III/IV}$ active species are particularly critical to enable OER and simultaneously inspires us that the observed Au-SPR-excitation-enhanced OER catalysis over $Ni(OH)_2$–Au might be essentially related to the increase in $Ni^{II}/Ni^{III/IV}$ transformation.

Herein, the redox behaviors of $Ni^{II}/Ni^{III/IV}$ were investigated. In Figure 3a, the oxidation peaks of Ni^{II} to $Ni^{III/IV}$ are clearly presented at around 1.42 V vs RHE. According to the method reported previously,[9,23] the extent of the $Ni^{II}/Ni^{III/IV}$ transformation could be qualitatively determined by the integrated oxidation peak areas (for details, see Table S1, SI). As seen from the inset of Figure 3a, when the $Ni(OH)_2$–Au electrode is irradiated by the 532 nm laser, the ratio of oxidized Ni indeed shows to be dramatically increased, thus potentially providing more active sites for OER catalysis. This result is in good agreement with the observed much enhanced activity upon illumination (Figure 2a). Moreover, a high wavelength dependence between such irradiation-enhanced $Ni^{II}/Ni^{III/IV}$ transformation and Au SPR absorption is further confirmed (Figure S16, SI). As a reference, the Au-free $Ni(OH)_2$ electrode, which shows negligible current response to the laser irradiation, accordingly exhibits ignorable light-enhanced $Ni^{II}/Ni^{III/IV}$ transformation. Therefore, it could be concluded that the plasmonic excitation of Au nanoparticles enhances the oxidation of Ni^{II} to $Ni^{III/IV}$ active sites in $Ni(OH)_2$–Au catalysts and subsequently much increases the OER catalysis.

Why does the SPR effect of Au nanoparticles enable the enhanced generation of $Ni^{III/IV}$ active species in the $Ni(OH)_2$–Au electrode during catalysis? To this end, the SPR-excitation-mediated electron transfer process should be carefully explored. It has been well-documented that the photon-induced plasmonic excitation of Au nanoparticles is accompanied by the formation and transfer of hot electrons to nearby electron acceptors and concurrently leaves the Au nanoparticles

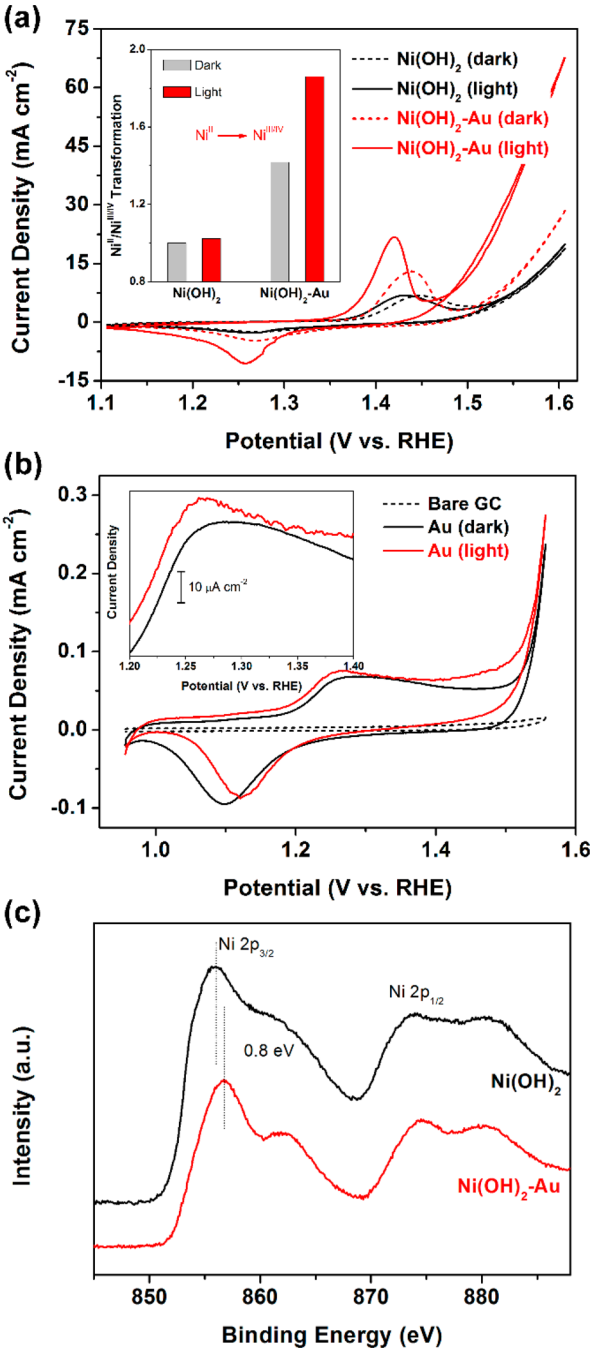

Figure 3. (a) Cyclic voltammetry curves recorded with and without 532 nm laser irradiation for $Ni(OH)_2$ nanosheets and $Ni(OH)_2$–Au hybrids. The inset in part a displays the normalized transformation of $Ni^{II}/Ni^{III/IV}$ on the basis of $Ni(OH)_2$ nanosheets (dark). (b) Cyclic voltammetry curves recorded with and without 532 nm laser irradiation for Au nanoparticles supported by the GC electrode. The inset in part b shows the enlarged oxidation peaks of Au between 1.20 and 1.40 V vs RHE. (c) High-resolution Ni 2p XPS spectra of $Ni(OH)_2$ nanosheets and $Ni(OH)_2$–Au hybrids.

positively charged.[10a,11h,24] Therefore, it could be reasonably speculated that this process may cause a positive effect on the oxidation of Au but a negative effect on the reduction. Accordingly, we performed the photoelectrochemical voltammetry to confirm the hot-electron transfer over Au nanoparticles. As shown in Figure 3b, the anodic peak around 1.25 V and the cathodic peak around 1.10 V can be assigned to the

DOI: 10.1021/jacs.6b05190
J. Am. Chem. Soc. 2016, 138, 9128–9136

oxidation and the reduction of Au nanoparticles, respectively.[7a,25] Upon 532 nm laser irradiation, the excited Au nanoparticles indeed exhibit an enhanced oxidation current and a depressed reduction current. This result directly indicates the occurrence of SPR-excitation-induced hot-electron injection on Au nanoparticles under laser irradiation. The additional evidence for this conclusion can be also the observation of the activated OER performance of Au nanoparticles via SPR excitation (Figure 2a).

To evaluate the hot-electron-transfer process more accurately, the femtosecond-resolved transient absorption (TA) spectroscopic analysis was further conducted. The TA spectra excited at 470 nm for Au nanoparticles with and without the carbon supporter are shown in parts a and b of Figure S17 (SI), respectively, in which both spectra exhibit a strong plasmon band bleaching signal at λ = 540 nm and a positive absorption at λ = 490 nm. This is indicative of the generation of hot electrons on Au nanoparticles under the plasmonic excitation.[26] Figure S17c (SI) shows the comparison of the kinetics probed at 540 nm (corresponding to the plasmon bleach) for Au and Au/carbon. It can be clearly seen that, in comparison with the sample without carbon, the Au/carbon exhibits a much slower hot-electron recovery. This result evidently suggests that hot electrons induced by plasmonic excitation could be transferred from Au nanoparticles to carbon and therefore affords an increased lifetime.[26b,d] Since the surface plasmons on Au nanoparticles could also decay radiatively by emission of luminescence, the photoluminescence (PL) measurements were also performed to confirm the above hot-electron-transfer process as previously reported.[11h,24,27] As shown in Figure S17d (SI), under the excitation of a 390 nm laser, Au nanoparticles exhibit a strong PL spectrum. Importantly, after the introduction of carbon, the PL intensity of Au nanoparticles dramatically decreases. This quenching effect agrees well with other reports and reflects the hot-electron transfer from Au nanoparticles to carbon.[11h,24]

Simultaneously, due to the high electronegativity of Au, the introduction of Au nanoparticles into the $Ni(OH)_2$ nanosheets could give rise to a small charge transfer from $Ni(OH)_2$ to Au.[5g,6b] This would make $Ni(OH)_2$ more easily oxidized and facilitate the formation of active $Ni^{III/IV}$ species to some extent, as we observed, and consequently cause a slightly enhanced OER activity (Figure 2a; see the activity comparison between $Ni(OH)_2$–Au and $Ni(OH)_2$ in the dark).[6b] Such intrinsic charge transfer is confirmed by the XPS analysis [Figures 3c and S18a (SI)],[7b] which shows that the electron binding energy of Ni 2p increases ~0.8 eV after loading with Au nanoparticles, and meanwhile, the Au 4f peaks of $Ni(OH)_2$–Au are negatively shifted compared to those of the pure Au nanoparticles. A consistent conclusion is also obtained from the similar positive shift in energy loss for the corresponding electron energy loss spectra (Figure S18b, SI).[28] When the $Ni(OH)_2$–Au catalysts were irradiated by the laser, the as-confirmed Au-SPR-induced hot-electron injection would leave positive holes as electron trappers on the Au nanoparticle surface, which is believed to significantly amplify the intrinsic electron transfer from $Ni(OH)_2$ to Au. Thus, the remarkable enhancement in $Ni^{III/IV}$ generation as shown in Figure 3a could be reasonably speculated.

To collect the direct evidence supporting the above-proposed enhancing effect of SPR excitation on electron transfer from $Ni(OH)_2$ to Au, the electron spin resonance (ESR) spectra of $Ni(OH)_2$–Au hybrids were further measured with and without laser irradiation (532 nm). As references, pure $Ni(OH)_2$ nanosheets, commercial nickel(II) oxide (NiO), and nickel(III) oxide (Ni_2O_3) were also analyzed. In Figures 4 and S19 (SI), though the stoichiometric nickel oxidation state in the as-prepared $Ni(OH)_2$ nanosheets is 2, the $Ni(OH)_2$ shows an ESR spectrum similar to that of commercial Ni_2O_3 rather than NiO (NiO possesses an antiferromagnetic feature[29]) and exhibits three broad paramagnetic absorption signals with g ≈ 2.208, 4.210, and 9.438, indicating the Ni^{III} feature.[30] This might be relative to the trace surface oxidation of $Ni(OH)_2$ nanosheets in air, as proved by the XPS results (Figure S20, SI). Loading with Au nanoparticles does not lead to any detectable difference in the ESR signals belonging to Ni^{III} in $Ni(OH)_2$. It is likely that the variation in the electronic structure of Ni cations in $Ni(OH)_2$ after Au loading is so small that it is beyond the detectable limitation of ESR analysis, reflecting the weakness of the intrinsic charge transfer from $Ni(OH)_2$ to Au. In sharp contrast, when the ESR spectrum of $Ni(OH)_2$–Au was measured under irradiation, the signals of Ni^{III} are evidently increased as compared to dark conditions. This result not only indicates that the holes generated by SPR excitation on the Au surface are capable of oxidizing the Ni^{II} cations in $Ni(OH)_2$ but also suggests that the SPR effect remarkably enhances the electron transfer from $Ni(OH)_2$ to Au and finally results in the more efficient generation of $Ni^{III/IV}$ active sites for OER catalysis. This conclusion is quite consistent with aforementioned voltammetry analysis (Figure 3a). As a control, the ESR spectrum of bare $Ni(OH)_2$ nanosheets was also analyzed under the laser irradiation, and no obvious photoresponse was shown, as expected (Figure S21, SI).

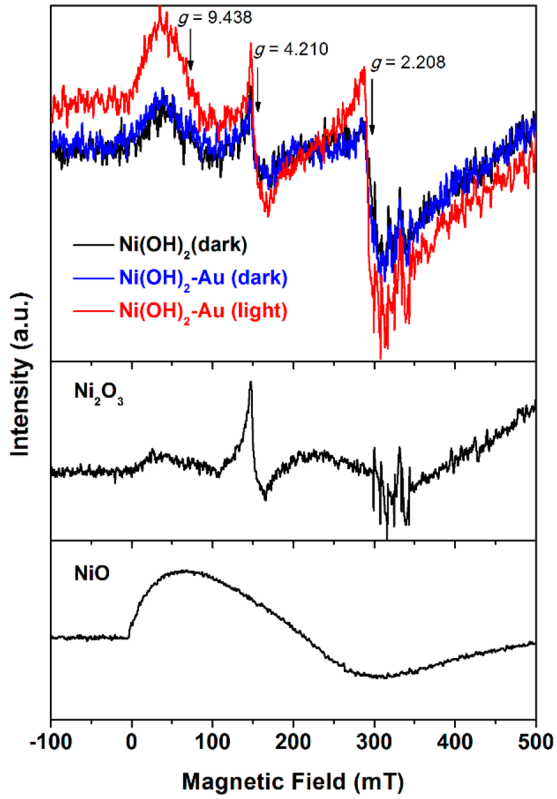

Figure 4. ESR spectra of bare $Ni(OH)_2$ nanosheets and $Ni(OH)_2$–Au hybrids. Commercial NiO and Ni_2O_3 were also tested (in the dark) for comparison. "Light" indicates "under laser irradiation".

DOI: 10.1021/jacs.6b05190
J. Am. Chem. Soc. 2016, 138, 9128–9136

Therefore, we propose the following mechanism to be responsible for the observed enhancements in active $Ni^{III/IV}$ species generation (Figure 3a) and subsequent OER catalysis (Figure 2) over the $Ni(OH)_2$–Au electrode under the 532 nm laser irradiation (Figure 5). Upon laser irradiation, hot

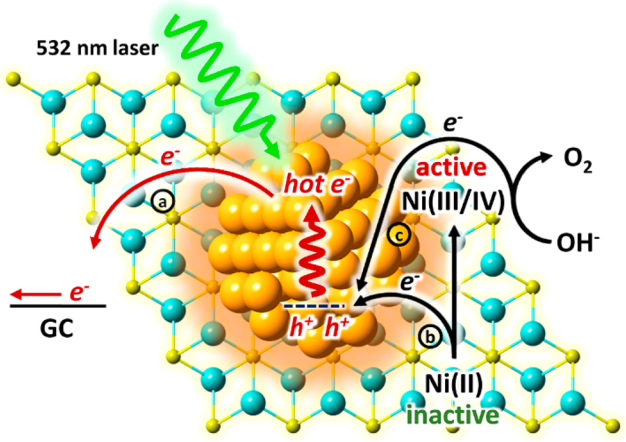

Figure 5. Schematic electron transfer paths likely to occur in the $Ni(OH)_2$–Au electrode under 532 nm laser irradiation responsible for the OER catalysis. The dashed line indicates the Fermi level of the Au nanoparticle. Light yellow, cyan, and orange balls correspond to Ni, O, and Au atoms, respectively. Hydrogen atoms are omitted for clarity in the structure of $Ni(OH)_2$.

electrons (near the Fermi level) in Au nanoparticles are excited to surface plasmon states and then transferred to the GC substrate electrode across the Ohmic interface between Au and GC with the assistance of external voltage (Figure 5a),[10a,31] which leaves the energetic holes on Au nanoparticles to function as effective electron trappers to capture electrons from $Ni(OH)_2$,[11a,b,32] remarkably enhancing the intrinsic charge transfer from $Ni(OH)_2$ to Au and casting two profound impacts on the OER catalysis: (i) facilitating the oxidation of inactive Ni^{II} to active $Ni^{III/IV}$, enabling OER (Figure 5b and Scheme S1, step 1 in the SI), as evidenced by the voltammetry results in Figure 3a, and (ii) promoting $Ni^{III/IV}$ active sites to extract electrons from OH^- and accomplish the O_2 evolution (Figure 5c and Scheme S1, steps 2–4 in the SI). The latter point could find support from Figures S7 and S8 (SI), which both show that removing laser irradiation leads to an abrupt and remarkable suppression of O_2 evolution. Since Au is not a good OER catalysts as compared to $Ni(OH)_2$ (as shown in Figure 2 and the previous reports[6b,7a]), the contribution from the direct electrochemical water oxidation by the SPR-induced holes on the Au nanoparticle could be ignored in the case using $Ni(OH)_2$–Au hybrids as catalysts, but it should be essential for the light-enhanced Au nanoparticle OER catalysis (Figure 2).

On the other hand, in contrast to the case under dark conditions (Figure S22, SI), the photodriven SPR excitation of Au nanoparticles is imagined to behave like an electron pump, significantly accelerating the electron transfer in the $Ni(OH)_2$–Au electrode via the hot-electron injection. This could be clearly elucidated by the electrochemical impedance spectroscopy (EIS) analysis. As shown in Figure S23 (SI), both the impedance spectra, measured in the dark and under laser irradiation, respectively, can be modeled using a modified Randles circuit consisting of a series resistance (R_S), a charge transfer resistance (R_{ct}), a mass transfer resistance (R_{mt}), and two constant phase elements (CPE) in parallel with the R.[12] According to the fitting results, remarkably, upon laser irradiation, the R_{ct} of $Ni(OH)_2$–Au shows a more than 30% decrease. This suggests that the irradiation-driven plasmonic excitation of Au leads to the higher charge transport efficiency in the electrode, agreeing well with our hypothesis.

On basis of the discussion above, we therefore propose that the light-induced substantial improvement in water oxidation over $Ni(OH)_2$–Au hybrid catalysts might be a result of the synergy of the enhanced generation of $Ni^{III/IV}$ active species and the improved charge transfer, which both are derived from the plasmonic excitation of Au nanoparticles. Furthermore, apart from $Ni(OH)_2$, such irradiation-enhanced OER catalysis could also be observed over cobalt oxide (CoO)–Au and iron oxyhydroxide (FeOOH)–Au catalysts, as shown in Figure S24 (SI), suggesting the generality of this strategy. More importantly, all these results and discussions presented above show that the electron withdrawing or donating generated on plasmonic metal nanostructures (e.g., Au nanoparticles) due to the SPR excitation might offer a universal strategy to modify the electronic structure of contiguous OER catalysts, thus activating their OER catalysis significantly and leading to more efficient oxygen evolution.

To clarify the possibility of the practical applications of this approach, we further conducted the OER catalysis with AM 1.5G illumination (equipped with a homemade light condenser) as light source (for the setup, see Figure S25, SI). As shown in Figure S26b (SI), under the illumination, a much enhanced OER performance was also detected over the $Ni(OH)_2$–Au catalysts, though the enhancement is lower than that with the laser as the light source, which leads to the overpotential at 10 mA cm^{-2} to be decreased to 300 mV (Figure S26c, SI) and meanwhile achieves a nearly double current density at 1.60 V vs RHE (Figure S26d, SI). Furthermore, at the current density of 50 mA cm^{-2}, the solar energy conversion efficiency was calculated to be 0.22% (for calculation details, please see the SI). These results clearly imply that sunlight could be used as the light source in the present system to realize much improved electrocatalytic OER catalysis and also suggest that the approach explored here could be potentially applied in practice.

4. CONCLUSION

In conclusion, we report $Ni(OH)_2$ nanosheets decorated with plasmonic Au nanoparticles [$Ni(OH)_2$–Au] as catalysts for electrochemical water oxidation and find that the corresponding OER performance could be significantly improved by the resonant surface plasmon excitation generated on illuminated plasmonic Au nanoparticles. Upon irradiation, the overpotential at the current density of 10 mA cm^{-2} is reduced from 330 to 270 mV, and the Tafel slope is decreased from 43 to 35 mV dec^{-1}; particularly, a more than 4-fold enhancement in both mass activity and TOF is shown. As evidenced by photoelectrochemical analysis and TA and ESR results, this improvement relies on the synergy of the enhanced generation of $Ni^{III/IV}$ active species and the improved charge transfer. Furthermore, we also show that the basic mechanism in the study should be universal, and the similar principles could contribute to the creation of other OER electrocatalysts (such as CoO–Au and FeOOH–Au) with more efficient activity through the plasmon activation (Figure S24, SI). It is believed that these findings potentially provide new avenues toward

DOI: 10.1021/jacs.6b05190
J. Am. Chem. Soc. 2016, 138, 9128–9136

more-energy-efficient catalytic water oxidation and related energy conversion systems.

5. EXPERIMENTAL SECTION

General. All chemical reagents were supplied by Wako and Sigma-Aldrich and were used without further purification. Ultrapure water (18.2 MΩ·cm resistivity at 25 °C) was used in all experiments.

Preparation of $Ni(OH)_2$ Nanosheets. $Ni(OH)_2$ nanosheets were prepared through a modified solvothermal method.[12] Typically, 0.7 g of $Ni(NO_3)_2{\cdot}6H_2O$ was first dissolved into 48 mL of ethanol to form a clear green solution under magnetic stirring. Then, 4.8 mL of oleylamine was quickly injected into the solution, followed by the further addition of 24 mL of ethanol. After being stirred for 30 min, the mixture solution was transferred into a 120 mL Teflon-lined stainless autoclave and heated to 190 °C for 16 h. Finally, the resulting precipitates were collected and washed with cyclohexane, distilled water, and ethanol thoroughly and dried at 50 °C under vacuum.

Preparation of Au Nanoparticles. Au nanoparticles were prepared by adding 3 mL of ice-cold $NaBH_4$ solution (0.1 M) to 100 mL of 0.25 mM $HAuCl_4$ under vigorous stirring for 5 min. The color of the solution changed immediately from yellow to wine red, indicating the formation of Au nanoparticles. Before being used, the Au colloid solution was aged in the dark at least 12 h to allow the hydrolysis of unreacted $NaBH_4$.

Self-Assembly of $Ni(OH)_2$ Nanosheets with Au Nanoparticles. $Ni(OH)_2$ nanosheets were assembled with Au nanoparticles through the electrostatic interaction. $Ni(OH)_2$ nanosheets (10 mg) were dispersed in 10 mL of ethanol under vigorous stirring. Then, 10 mL of the as-prepared Au colloid solution was added dropwise. After stirring for 3 h, the resulting sample [denoted as $Ni(OH)_2$–Au] was collected and washed with water. The total Au content in $Ni(OH)_2$–Au was measure to be 3.5 wt % by an inductively coupled plasma optical emission spectroscopy (SII Nano Technology Inc., model SPS3520UV-DD) technique. When 5, 20, and 30 mL of Au colloid solutions were used, the Au contents were determined to be 1.8, 6.4, and 8.9 wt %, respectively.

Characterization. TEM and HR-TEM were conducted on a Tecnai G2 F30 S-Twin electron microscope operated at 300 kV. HAADF-STEM images and EDS mapping images were taken on a JEOL 2100F microscope. SEM images were recorded on a Hitachi S4800 microscope. Powder XRD was performed on an X'Pert PRO diffractometer with Cu Kα radiation (PANalytical). A UV–visible spectrophotometer (UV-2600, Shimadzu Corp.) was used to measure the absorption spectra of the as-prepared samples. PL spectra excited at 390 nm were recorded on a Spex Fluorolog-3 spectrofluorometer. The femtosecond-resolved transient absorption data were obtained using a Helios transient absorption spectrometer (Ultrafast Systems) (for details, see the SI). N_2 adsorption–desorption experiments were performed at 77 K to examine the Brunauer–Emmett–Teller surface area (BELsorp II mini, BEL Japan Inc.). Before measuring, the samples were degassed in a vacuum at 60 °C for 12 h. Surface chemical analysis was performed by XPS (PHI Quantera SXM, ULVAC-PHI Inc.). The surface potentials of the samples dispersed in a water/ethanol (1/1 volume ratio) solution were determined using the Delsa Nano ζ-potential and submicron particle size analyzer (Beckman Coulter). ESR spectra were recorded on a JES-FA200 electron spin resonance spectrometer operating at about 9.0 GHz at room temperature. The magnetic field was calibrated with Mn(II) in MgO.

Electrochemical Measurements. All the electrochemical measurements were performed in a three-electrode system using a CHI ALS/CH-650A instrument at room temperature. Pt wire and Ag/AgCl (saturated KCl) were used as counter and reference electrodes, respectively. The electrolyte was 1.0 M KOH aqueous solution (purged by pure O_2). The working electrodes for $Ni(OH)_2$ and $Ni(OH)_2$–Au were made by drop-casting 7.5 μL of catalyst dispersion [2.5 mg of catalyst dispersed in 1 mL of 3:1 v/v water/isopropyl alcohol mixed solvent containing 20 μL of Nafion solution (5 wt %)] onto a glassy carbon (GC) electrode (3 mm diameter), leading to the catalyst loading of ~0.265 mg cm^{-2}. Linear sweep voltammetry and cyclic voltammetry curves were measured at room temperature and 2000 rpm, with a sweep rate of 10 mV s^{-1}. Electrochemical impedance spectra were recorded at an applied potential of 0.50 V vs Ag/AgCl over the frequency range from 1 MHz to 0.1 Hz with an amplitude of applied voltage of 5 mV. The output power of the 532 nm laser irradiation was 1.2 W.

Calculation Method. The mass activity, specific activity, and TOF of the catalysts are calculated as follows:[12]

$$\text{mass activity} = \frac{j}{m} \tag{1}$$

$$\text{specific activity} = \frac{j}{10mS_{\text{BET}}} \tag{2}$$

$$\text{TOF} = \frac{jS}{4Fn} \tag{3}$$

Here, j is the measured current density (mA cm^{-2}), m is the catalyst loading (mg cm^{-2}), S_{BET} indicates the BET surface area of the catalyst, S is the surface area of the GC electrode, the number 4 in the TOF calculation means 4 electrons required for one O_2 molecule evolution, F is Faraday's constant (96485.3 C mol^{-1}), and n is the moles of metal atom on the electrode.

■ ASSOCIATED CONTENT

Supporting Information

The Supporting Information is available free of charge on the ACS Publications website at DOI: 10.1021/jacs.6b05190.

SEM and TEM images, ζ-potential measurements, BET surface area measurements, EDS spectrum, XRD patterns, UV–vis absorption spectra, XPS spectra, EELS spectra, polarization curves, I–t curves, details of transient absorption measurements, ESR spectra, EIS Nyquist plots, a table listing the $Ni^{II}/Ni^{III/IV}$ transformation ratios, a table presenting a comparison of the OER catalytic performance of $Ni(OH)_2$–Au to that of recently reported state-of-the-art OER catalysts, and a figure showing the OER performance of CoO–Au and FeOOH–Au catalysts with laser irradiation (Figures S1–S26, Tables S1 and S2, and Scheme S1) (PDF)

■ AUTHOR INFORMATION

Corresponding Authors

*ZHANG.Huabin@nims.go.jp

*Jinhua.YE@nims.go.jp

Notes

The authors declare no competing financial interest.

■ ACKNOWLEDGMENTS

This research received financial support from the World Premier International Research Center Initiative (WPI Initiative) on Materials Nanoarchitectonics (MANA), MEXT (Japan), the National Basic Research Program of China (973 Program, 2014CB239301), Mitsubishi Foundation, and the JSPS KAKENHI (Grant No. 15K00591, 15F15070, and 16F16049). The author thanks Prof. Hidenori Noguchi from NIMS for helpful discussions.

■ REFERENCES

(1) (a) Lewis, N. S.; Nocera, D. G. *Proc. Natl. Acad. Sci. U. S. A.* **2006**, *103*, 15729. (b) Kudo, A.; Miseki, Y. *Chem. Soc. Rev.* **2009**, *38*, 253. (c) White, J. L.; Baruch, M. F.; Pander Iii, J. E.; Hu, Y.; Fortmeyer, I. C.; Park, J. E.; Zhang, T.; Liao, K.; Gu, J.; Yan, Y.; Shaw, T. W.; Abelev, E.; Bocarsly, A. B. *Chem. Rev.* **2015**, *115*, 12888.

DOI: 10.1021/jacs.6b05190
J. Am. Chem. Soc. 2016, 138, 9128–9136

(2) (a) Walter, M. G.; Warren, E. L.; McKone, J. R.; Boettcher, S. W.; Mi, Q.; Santori, E. A.; Lewis, N. S. *Chem. Rev.* **2010**, *110*, 6446. (b) Hisatomi, T.; Kubota, J.; Domen, K. *Chem. Soc. Rev.* **2014**, *43*, 7520. (c) Zou, Z.; Ye, J.; Sayama, K.; Arakawa, H. *Nature* **2001**, *414*, 625. (d) Luo, J.; Im, J.-H.; Mayer, M. T.; Schreier, M.; Nazeeruddin, M. K.; Park, N.-G.; Tilley, S. D.; Fan, H. J.; Grätzel, M. *Science* **2014**, *345*, 1593. (e) Liu, G.; Wang, T.; Zhang, H.; Meng, X.; Hao, D.; Chang, K.; Li, P.; Kako, T.; Ye, J. *Angew. Chem., Int. Ed.* **2015**, *54*, 13561. (f) Tong, H.; Ouyang, S.; Bi, Y.; Umezawa, N.; Oshikiri, M.; Ye, J. *Adv. Mater.* **2012**, *24*, 229.

(3) (a) Chen, S.; Duan, J.; Jaroniec, M.; Qiao, S.-Z. *Adv. Mater.* **2014**, *26*, 2925. (b) Chen, S.; Duan, J.; Jaroniec, M.; Qiao, S. Z. *Angew. Chem., Int. Ed.* **2013**, *52*, 13567. (c) Zhao, Y.; Nakamura, R.; Kamiya, K.; Nakanishi, S.; Hashimoto, K. *Nat. Commun.* **2013**, *4*, 2390. (d) Suntivich, J.; May, K. J.; Gasteiger, H. A.; Goodenough, J. B.; Shao-Horn, Y. *Science* **2011**, *334*, 1383. (e) Martin, D. J.; Liu, G.; Moniz, S. J. A.; Bi, Y.; Beale, A. M.; Ye, J.; Tang, J. *Chem. Soc. Rev.* **2015**, *44*, 7808.

(4) Chen, D.; Chen, C.; Baiyee, Z. M.; Shao, Z.; Ciucci, F. *Chem. Rev.* **2015**, *115*, 9869.

(5) (a) Louie, M. W.; Bell, A. T. *J. Am. Chem. Soc.* **2013**, *135*, 12329. (b) Pintado, S.; Goberna-Ferrón, S.; Escudero-Adán, E. C.; Galán-Mascarós, J. R. *J. Am. Chem. Soc.* **2013**, *135*, 13270. (c) Trotochaud, L.; Ranney, J. K.; Williams, K. N.; Boettcher, S. W. *J. Am. Chem. Soc.* **2012**, *134*, 17253. (d) Trotochaud, L.; Young, S. L.; Ranney, J. K.; Boettcher, S. W. *J. Am. Chem. Soc.* **2014**, *136*, 6744. (e) Wu, L.; Li, Q.; Wu, C. H.; Zhu, H.; Mendoza-Garcia, A.; Shen, B.; Guo, J.; Sun, S. *J. Am. Chem. Soc.* **2015**, *137*, 7071. (f) Niu, K.-Y.; Lin, F.; Jung, S.; Fang, L.; Nordlund, D.; McCrory, C. C. L.; Weng, T.-C.; Ercius, P.; Doeff, M. M.; Zheng, H. *Nano Lett.* **2015**, *15*, 2498. (g) Yeo, B. S.; Bell, A. T. *J. Am. Chem. Soc.* **2011**, *133*, 5587. (h) McCrory, C. C. L.; Jung, S.; Ferrer, I. M.; Chatman, S. M.; Peters, J. C.; Jaramillo, T. F. *J. Am. Chem. Soc.* **2015**, *137*, 4347. (i) Smith, R. D. L.; Prévot, M. S.; Fagan, R. D.; Trudel, S.; Berlinguette, C. P. *J. Am. Chem. Soc.* **2013**, *135*, 11580. (j) Chen, S.; Qiao, S.-Z. *ACS Nano* **2013**, *7*, 10190. (k) Liang, H.; Meng, F.; Cabán-Acevedo, M.; Li, L.; Forticaux, A.; Xiu, L.; Wang, Z.; Jin, S. *Nano Lett.* **2015**, *15*, 1421.

(6) (a) Juodkazis, K.; Juodkazytė, J.; Vilkauskaitė, R.; Jasulaitienė, V. *J. Solid State Electrochem.* **2008**, *12*, 1469. (b) Yeo, B. S.; Bell, A. T. *J. Phys. Chem. C* **2012**, *116*, 8394. (c) Bediako, D. K.; Lassalle-Kaiser, B.; Surendranath, Y.; Yano, J.; Yachandra, V. K.; Nocera, D. G. *J. Am. Chem. Soc.* **2012**, *134*, 6801. (d) Bediako, D. K.; Surendranath, Y.; Nocera, D. G. *J. Am. Chem. Soc.* **2013**, *135*, 3662. (e) Xu, K.; Chen, P.; Li, X.; Tong, Y.; Ding, H.; Wu, X.; Chu, W.; Peng, Z.; Wu, C.; Xie, Y. *J. Am. Chem. Soc.* **2015**, *137*, 4119. (f) Wang, J.; Li, K.; Zhong, H.-x.; Xu, D.; Wang, Z.-l.; Jiang, Z.; Wu, Z.-j.; Zhang, X.-b. *Angew. Chem., Int. Ed.* **2015**, *54*, 10530.

(7) (a) Zhuang, Z.; Sheng, W.; Yan, Y. *Adv. Mater.* **2014**, *26*, 3950. (b) Gao, M.-R.; Xu, Y.-F.; Jiang, J.; Zheng, Y.-R.; Yu, S.-H. *J. Am. Chem. Soc.* **2012**, *134*, 2930.

(8) (a) Balasubramanian, M.; Melendres, C. A.; Mini, S. *J. Phys. Chem. B* **2000**, *104*, 4300. (b) Guerlou-Demourgues, L.; Fournès, L.; Delmas, C. *J. Electrochem. Soc.* **1996**, *143*, 3083. (c) Lyons, M. E. G.; Brandon, M. P. *J. Electroanal. Chem.* **2010**, *641*, 119.

(9) Tang, C.; Wang, H.-S.; Wang, H.-F.; Zhang, Q.; Tian, G.-L.; Nie, J.-Q.; Wei, F. *Adv. Mater.* **2015**, *27*, 4516.

(10) (a) Linic, S.; Christopher, P.; Ingram, D. B. *Nat. Mater.* **2011**, *10*, 911. (b) Clavero, C. *Nat. Photonics* **2014**, *8*, 95.

(11) (a) Lee, J.; Mubeen, S.; Ji, X.; Stucky, G. D.; Moskovits, M. *Nano Lett.* **2012**, *12*, 5014. (b) Mubeen, S.; Lee, J.; Singh, N.; Kramer, S.; Stucky, G. D.; Moskovits, M. *Nat. Nanotechnol.* **2013**, *8*, 247. (c) Mubeen, S.; Hernandez-Sosa, G.; Moses, D.; Lee, J.; Moskovits, M. *Nano Lett.* **2011**, *11*, 5548. (d) Liu, G.; Wang, T.; Zhou, W.; Meng, X.; Zhang, H.; Liu, H.; Kako, T.; Ye, J. *J. Mater. Chem. C* **2015**, *3*, 7538. (e) Shi, Y.; Wang, J.; Wang, C.; Zhai, T.-T.; Bao, W.-J.; Xu, J.-J.; Xia, X.-H.; Chen, H.-Y. *J. Am. Chem. Soc.* **2015**, *137*, 7365. (f) Bian, Z.; Tachikawa, T.; Kim, W.; Choi, W.; Majima, T. *J. Phys. Chem. C* **2012**, *116*, 25444. (g) Bian, Z.; Tachikawa, T.; Zhang, P.; Fujitsuka, M.; Majima, T. *J. Am. Chem. Soc.* **2014**, *136*, 458. (h) Zheng, Z.; Tachikawa, T.; Majima, T. *J. Am. Chem. Soc.* **2015**, *137*, 948.

(12) Gao, M.; Sheng, W.; Zhuang, Z.; Fang, Q.; Gu, S.; Jiang, J.; Yan, Y. *J. Am. Chem. Soc.* **2014**, *136*, 7077.

(13) Liu, L.; Ouyang, S.; Ye, J. *Angew. Chem., Int. Ed.* **2013**, *52*, 6689.

(14) (a) Xu, L.; Ding, Y.-S.; Chen, C.-H.; Zhao, L.; Rimkus, C.; Joesten, R.; Suib, S. L. *Chem. Mater.* **2008**, *20*, 308. (b) Jeevanandam, P.; Koltypin, Y.; Gedanken, A. *Nano Lett.* **2001**, *1*, 263.

(15) Oliver-Tolentino, M. A.; Vázquez-Samperio, J.; Manzo-Robledo, A.; González-Huerta, R. d. G.; Flores-Moreno, J. L.; Ramírez-Rosales, D.; Guzmán-Vargas, A. *J. Phys. Chem. C* **2014**, *118*, 22432.

(16) Naya, S.-i.; Niwa, T.; Kume, T.; Tada, H. *Angew. Chem., Int. Ed.* **2014**, *53*, 7305.

(17) Tian, Y.; Tatsuma, T. *J. Am. Chem. Soc.* **2005**, *127*, 7632.

(18) Huang, J.; Chen, J.; Yao, T.; He, J.; Jiang, S.; Sun, Z.; Liu, Q.; Cheng, W.; Hu, F.; Jiang, Y.; Pan, Z.; Wei, S. *Angew. Chem., Int. Ed.* **2015**, *54*, 8722.

(19) Chen, P.; Xu, K.; Zhou, T.; Tong, Y.; Wu, J.; Cheng, H.; Lu, X.; Ding, H.; Wu, C.; Xie, Y. *Angew. Chem., Int. Ed.* **2016**, *55*, 2488.

(20) (a) Gunnarsson, L.; Rindzevicius, T.; Prikulis, J.; Kasemo, B.; Käll, M.; Zou, S.; Schatz, G. C. *J. Phys. Chem. B* **2005**, *109*, 1079. (b) Liu, Z.; Hou, W.; Pavaskar, P.; Aykol, M.; Cronin, S. B. *Nano Lett.* **2011**, *11*, 1111. (c) Christopher, P.; Xin, H.; Marimuthu, A.; Linic, S. *Nat. Mater.* **2012**, *11*, 1044.

(21) Sakamoto, H.; Ohara, T.; Yasumoto, N.; Shiraishi, Y.; Ichikawa, S.; Tanaka, S.; Hirai, T. *J. Am. Chem. Soc.* **2015**, *137*, 9324.

(22) Gong, M.; Li, Y.; Wang, H.; Liang, Y.; Wu, J. Z.; Zhou, J.; Wang, J.; Regier, T.; Wei, F.; Dai, H. *J. Am. Chem. Soc.* **2013**, *135*, 8452.

(23) Burke, M. S.; Enman, L. J.; Batchellor, A. S.; Zou, S.; Boettcher, S. W. *Chem. Mater.* **2015**, *27*, 7549.

(24) Zheng, Z.; Tachikawa, T.; Majima, T. *J. Am. Chem. Soc.* **2014**, *136*, 6870.

(25) Schmidt, T. J.; Stamenkovic, V.; Arenz, M.; Markovic, N. M.; Ross, P. N., Jr *Electrochim. Acta* **2002**, *47*, 3765.

(26) (a) Ahmadi, T. S.; Logunov, S. L.; El-Sayed, M. A. *J. Phys. Chem.* **1996**, *100*, 8053. (b) Mahmoud, M. A.; Qian, W.; El-Sayed, M. A. *Nano Lett.* **2011**, *11*, 3285. (c) Wu, K.; Rodríguez-Córdoba, W. E.; Yang, Y.; Lian, T. *Nano Lett.* **2013**, *13*, 5255. (d) Huang, H.; Zhang, L.; Lv, Z.; Long, R.; Zhang, C.; Lin, Y.; Wei, K.; Wang, C.; Chen, L.; Li, Z.-Y.; Zhang, Q.; Luo, Y.; Xiong, Y. *J. Am. Chem. Soc.* **2016**, *138*, 6822.

(27) (a) Tcherniak, A.; Dominguez-Medina, S.; Chang, W.-S.; Swanglap, P.; Slaughter, L. S.; Landes, C. F.; Link, S. *J. Phys. Chem. C* **2011**, *115*, 15938. (b) Dulkeith, E.; Niedereichholz, T.; Klar, T. A.; Feldmann, J.; von Plessen, G.; Gittins, D. I.; Mayya, K. S.; Caruso, F. *Phys. Rev. B: Condens. Matter Mater. Phys.* **2004**, *70*, 205424.

(28) (a) Ma, X.; Liu, J.; Liang, C.; Gong, X.; Che, R. *J. Mater. Chem. A* **2014**, *2*, 12692. (b) Goris, B.; Turner, S.; Bals, S.; Van Tendeloo, G. *ACS Nano* **2014**, *8*, 10878.

(29) Nkosi, S. S.; Yalisi, B.; Motaung, D. E.; Keartland, J.; Sideras-Haddad, E.; Forbes, A.; Mwakikunga, B. W. *Appl. Surf. Sci.* **2013**, *265*, 860.

(30) (a) Stoyanova, R.; Zhecheva, E.; Alcántara, R.; Tirado, J. L. *J. Phys. Chem. B* **2004**, *108*, 4053. (b) Zhao, Y.; Wang, Q.; Bian, T.; Yu, H.; Fan, H.; Zhou, C.; Wu, L.-Z.; Tung, C.-H.; O'Hare, D.; Zhang, T. *Nanoscale* **2015**, *7*, 7168.

(31) (a) Park, J. Y.; Baker, L. R.; Somorjai, G. A. *Chem. Rev.* **2015**, *115*, 2781. (b) Zheng, B. Y.; Zhao, H.; Manjavacas, A.; McClain, M.; Nordlander, P.; Halas, N. J. *Nat. Commun.* **2015**, *6*, 7797.

(32) Yu, S.; Kim, Y. H.; Lee, S. Y.; Song, H. D.; Yi, J. *Angew. Chem., Int. Ed.* **2014**, *53*, 11203.

DOI: 10.1021/jacs.6b05190
J. Am. Chem. Soc. 2016, 138, 9128−9136